

Stress Development and Impurity Segregation during Oxidation of the Si(100) Surface

Daniel J. Cole,^{1*} Mike C. Payne,¹ and Lucio Colombi Ciacchi^{2,3}

¹*Theory of Condensed Matter Group, Cavendish Laboratory, University of Cambridge, J J Thomson Avenue, Cambridge CB3 0HE, UK*

²*Fraunhofer Institut für Werkstoffmechanik
Wöhlerstrasse 11, 79108 Freiburg, Germany*

³*Institut für Zuverlässigkeit von Bauteilen und Systemen, University of Karlsruhe, Kaiserstr. 12, 76131 Karlsruhe, Germany.*

Abstract

We have studied the segregation of P and B impurities during oxidation of the Si(100) surface by means of combined static and dynamical first-principles simulations based on density functional theory. In the bare surface, dopants segregate to chemically stable surface sites or to locally compressed subsurface sites. Surface oxidation is accompanied by development of tensile surface stress up to 2.9 N/m at a coverage of 1.5 monolayers of oxygen and by formation of oxidised Si species with charges increasing approximately linearly with the number of neighbouring oxygen atoms. Substitutional P and B defects are energetically unstable within the native oxide layer, and are preferentially located at or beneath the Si/SiO_x interface. Consistently, first-principles molecular dynamics simulations of native oxide formation on doped surfaces reveal that dopants avoid the formation of P–O and B–O bonds, suggesting a surface oxidation mechanism whereby impurities remain trapped at the Si/SiO_x interface. This seems to preclude a direct influence of impurities on the surface electrostatics and, hence, on the interactions with an external environment.

Keywords: Silicon surface; Impurity segregation; Oxidation; Surface stress; Boron; Phosphorous; Density functional calculations; Molecular dynamics

*To whom correspondence should be addressed;

e-mail: djc56@cam.ac.uk; phone: +44 (0)1223 337049; fax: +44 (0)1223 337356

1 Introduction

Interactions between Si-based microelectromechanical systems (MEMS) and their external environment are particularly important when their surfaces are in contact with an atmospheric or physiological milieu [1–4]. These interactions, largely of a non-covalent type, directly involve the natively oxidised Si surface and are thus strongly dependent on the distribution of charged species within the oxide layer. Such charge distributions may be affected by P and B dopants present in the Si bulk, if they tend to segregate into the oxide layer. Experimental and theoretical investigations [5,6] have established that P and B dopants segregate to the bare Si(100) surface in order to saturate dangling bonds and relieve strain in the Si lattice caused by size mismatch between the Si and dopant atoms. This combination of chemical and mechanical effects is expected to have a similar effect on impurity segregation into the thin native oxide surface layer that spontaneously forms on Si in the presence of oxygen. However, the detailed behaviour of such dopants during and after the oxidation process remains unclear and is currently the subject of a number of theoretical and experimental studies.

To address the issue of P segregation at the Si/SiO₂ interface, secondary ion mass spectroscopy (SIMS) has been widely used since it is capable of measuring compositions varying over several orders of magnitude as a function of depth. SIMS experiments reveal a decrease in P dopants of up to 50% on removal of the oxide layer, although the limited resolution in this case makes it impossible to determine whether these dopants were present in the oxide layer or at the interface [7]. On the other hand, inductively coupled plasma mass spectrometry measured just 2% of the initial dose of P atoms in the oxide layer after oxidation at 850 °C, with the majority shown by precise SIMS profiles piled up on the Si side of the interface [8]. These results are consistent with ab-initio simulations of such interfaces [9,10], in which it is found that P atoms avoid forming P–O bonds and are stable at threefold-coordinated defect sites, introduced during the oxidation process. At dopant concentrations above 0.01 nm⁻³, P atom pairs dominate with the interface accommodating the stress induced by bond deformation around the resulting defect.

In contrast to the Si/SiO₂ dielectric interface, there have been relatively few studies of impurity segregation at the interface between Si and its ultrathin native oxide. Such an interface contains a high concentration of defects (approximately 0.1 nm⁻² [9]), in the form of Si dangling bonds. SIMS experiments on a Si(100) native oxide report P segregation into the oxide layer at room temperature, which increases with annealing [11]. However, these measurements are taken at very high doping concentration (0.5 nm⁻³) and possible pile-up at the interface cannot be observed since the oxide layer is thin compared to the SIMS resolution. Auger electron spectroscopy data of a similar interface showed no spectral line corresponding to oxidised P [9].

There has been similar uncertainty among studies addressing the segregation behaviour of B impurities. A theoretical study of the Si/SiO₂ interface has proposed that B segregates to threefold-coordinated O vacancies in the oxide layer [12]. This is in response to experimental observations, reporting B diffusion through thin oxide layers during annealing of doped polysilicon [13], and SIMS profiles, revealing a sixfold excess of dopant atoms on the oxide side of the interface compared with the Si side [14]. On the other hand, recent reports suggest that surface peaks in B doped samples are artefacts of the SIMS analysis and are not confirmed by other techniques, known to be accurate at high doping concentration [15]. An energy-filtered transmission electron microscopy B profile of a clean Si(100) surface, doped at a concentration of 50 nm⁻², shows a peak at a depth of 60 Å [16]. The sample was shown to have a native oxide depth of approximately 15 Å, placing the B peak in the strained Si layer below the interface. This result is supported by high-resolution Rutherford backscattering spectroscopy, revealing that B is concentrated beneath the native oxide layer, formed after B implantation [17].

In this work, we aim to gain a basic understanding of the behaviour of P and B impurities during the formation of a native oxide layer on the Si(100) surface by performing combined static and dynamical first-principles simulations based on Density Functional Theory (DFT). Both the changes in Si coordination and the evolution of surface stress that occur during the formation of the native oxide layer on the bare p(2×2) reconstructed Si(100) surface will be investigated. We will then perform total energy calculations of

dopant substitution into various sites of bare and natively oxidised surface models. These static calculations are able to discriminate the thermodynamically stable dopant positions, but are limited by the number of configurations that may be investigated. Therefore, we complement the static approach by performing a series of first principles molecular dynamics (FPMD) simulations of the native oxide growth in the presence of surface dopants. Apart from the choice of the initial conditions, dynamical simulations are unbiased regarding the possible reaction paths, and reveal mechanistic details otherwise very difficult to access experimentally.

2 Methods

Total energy calculations are performed within the spin-polarised density functional theory, as implemented in the CASTEP code [18]. The gradient-corrected exchange correlation functional generated by Perdew, Burke and Ernzerhof [19] is employed, along with ultrasoft pseudopotentials to represent electron-ion interactions. Wave functions are expanded in plane waves up to a kinetic energy cut-off of 400 eV and a Gaussian smearing function of width 0.01 eV is applied to the electronic occupancies. With this choice of parameters, energy differences were found to converge to within 0.01 eV in selected test cases. The equilibrium bond length and cohesive energy of bulk Si were calculated to be 2.36 Å and 4.55 eV/atom respectively (the corresponding experimental values are 2.35 Å and 4.63 eV/atom [20]).

Molecular dynamical simulations [21] are performed as above, with a decreased plane wave energy cut-off of 300 eV and a time step of 1.5 fs. Most of the simulations are performed within the microcanonical ensemble. Where temperature constraints are required, a Nosé-Hoover thermostat with a 15 fs relaxation time is employed. Convergence criteria for determining minimum energy structures are set to 10^{-4} eV/atom for energy changes and 0.2 eV/Å and 0.01 Å for ionic forces and displacements respectively [22]. Atomic charges are computed via a Mulliken population analysis by projecting the ground state wave functions onto a basis consisting of s and p atomic orbitals [23].

Calculations on the Si(100) surface are performed using a periodically repeated 2×2 surface slab, sampling the Brillouin zone with two \mathbf{k} -points at $(0, \pm 0.25, 0.25)$ [24]. The surface model consists of 64 Si atoms arranged in eight layers and separated, in the x direction, by a vacuum layer equivalent to a further eight layers. The surface energy per atom of such a slab is defined as: $\gamma = (E_s - E_b)/n_s$, where E_s is the total ground state energy of the 64-atom surface model, E_b is the energy of a correspondent bulk model without any vacuum layer in the x direction, and n_s is the total number of surface atoms, 16 in this case.

3 Reconstruction of the (100) Surface

Cleaving a Si crystal along the (100) plane leaves each surface atom with two dangling bonds and a high charge density between the surface atoms (Fig. 1 (left)). To stabilise this structure, the surface atoms relax to form a series of alternating buckled dimers with a length of 2.35 Å and a buckling angle of 21° [25], known as a $p(2 \times 2)$ reconstruction (Fig. 1 (right)). The calculated surface energy, γ , of the reconstructed surface is 1.15 eV/atom [26], consistent with the energy required to break one bond per atom in bulk Si (1.14 eV/atom). A Mulliken population analysis reveals that the dimer reconstruction is accompanied by a redistribution of charge from the down dimer atom ($+0.14 e^-$) to the up atom ($-0.07 e^-$). This charge separation corresponds to a change of orbital hybridisation of the down and up dimer atoms from sp^3 to sp^2 and p^3 respectively, and has been shown to influence the pathway of oxygen chemisorption onto the bare surface [27].

The redistribution of electronic charge in the dangling bonds due to cleavage of the crystal in the (100) plane results in the presence of surface stress. For symmetry reasons, this is diagonal in the reference frame with axes parallel (\parallel) and perpendicular (\perp) to the dimer bonds. The two surface stress components are defined by the relations:

$$g_{\parallel} = \frac{1}{2}a\sigma_{\parallel}, \quad g_{\perp} = \frac{1}{2}a\sigma_{\perp},$$

where σ_{\parallel} and σ_{\perp} are the components of the stress tensor in the surface plane and a is the

height of the periodically repeated supercell [28]. In all calculations, the lattice parameter in the surface plane has been kept fixed to the bulk equilibrium value, and the stress component in the direction perpendicular to the surface was equal to zero.

The calculated g components of the bulk-terminated and p(2×2)-reconstructed Si(100) surface are summarised and compared to previous ab-initio simulations [29] in Table 1. As thoroughly discussed in [30], upon truncation of the bulk, the lone electrons tend to pull the surface atoms together to form dimers in the \parallel direction, resulting in high surface stress. This is largely reduced by formation of buckled dimers, but a residual tension remains, which is consistent with longer Si–Si bonds between atoms of the second and third layers beneath the dimer rows (Fig. 1). The bond angles at the down atom of each surface dimer are 120° , 119° and 118° , close to ideal sp^2 bonding. However, the bond angle between the up dimer atom and its two neighbours in the second layer is 99.5° , considerably larger than the 90° required for ideal p^3 bonding. This leads to an increased tensile stress component g_\perp in the p(2×2)-reconstructed surface with respect to the bulk truncated surface. Because of the positive stress anisotropy $g_\parallel - g_\perp$, alignment of the dimers in the direction of an externally applied compressive stress is expected to be energetically favourable. Indeed, experiments show that the number of domains compressed along the dimer bond increases at the expense of domains compressed perpendicularly to the bond [31].

4 Oxidation of the (100) Surface

We have seen in the previous section how structural features of the bare surface reconstruction are linked to redistribution of charge and surface stress, which we will show later to be important factors in controlling the segregation of impurities. Under normal atmospheric conditions, however, the Si surface is passivated by a thin oxide layer. In ref. [27], the oxidation of the Si(100) surface in a dry environment has been investigated by means of FPMD simulations. In good agreement with medium-energy ion scattering experiments [32], it was found that oxygen spontaneously adsorbs onto the bare surface up to a coverage of 1.5 monolayers (ML). At higher coverages, further oxide growth becomes limited by diffu-

sion of O₂ molecules to the reactive Si/SiO_x interface. The charged Si species in the final structure obtained in [27] after adsorption of six O₂ molecules range from Si⁺ to Si⁴⁺. We have performed a Mulliken analysis of this structure and found that the charges on the Si atoms increase approximately linearly with the number of nearest-neighbour O atoms, which act as electron acceptors (Fig. 2).

It is interesting to follow the development of stress in the partially oxidised surface at increasing oxygen coverage. We have fully relaxed all structures obtained after each FPMD simulation in [27], keeping the lower surface of the slab p(2×2)-reconstructed. The surface stress is then calculated as for the bare surface, except that, upon reaction with oxygen molecules, the symmetry of the dimer bonds is broken and shear components appear in the surface stress tensor. The total surface stress, g , may be defined as the basis invariant trace of the stress tensor, σ , computed in a supercell of height a :

$$g = \frac{1}{2}a \text{Tr}(\sigma_{\alpha\beta}) = \frac{1}{2}a(\sigma_{yy} + \sigma_{zz}).$$

In order to isolate the development of stress in the oxide layer at the top of our surface slab, the total surface stress of the bottom p(2×2) reconstructed surface (0.81 Nm⁻¹) is subtracted from all of the results.

The evolution of the total surface stress as successive O₂ molecules react with the surface is summarised in Fig. 3. The tensile stress initially present in the bare surface diminishes after reaction of the first molecule. In the final structure obtained, one O atom is adsorbed into a dimer bond, relieving the tension parallel to the bond direction (Fig. 3, red arrow). The second O atom binds between one up dimer atom and the neighbouring dimer (Fig. 3, blue arrow), breaking a bond to the second layer (black arrow) and relaxing the tension in the direction perpendicular to the dimer. Similar events lead to a further stress decrease after adsorption of a second and a third oxygen molecule. However, at a coverage of 1.25 ML, a backbone of alternating Si and O atoms develops in the surface oxide structure and extends over the neighbouring simulation cells due to the periodic boundary conditions employed. Formation of this continuous oxide layer, given the constraints exerted by the underlying crystalline bulk, results in a sudden appearance of a large tensile surface stress.

The obtained stress values are in reasonable agreement with the experimentally measured tensile stress of $+0.26 \text{ Nm}^{-1}$ per monolayer of oxygen [33]. An absolute comparison is difficult, since in [33] the authors assume a linear relationship between oxygen coverage and surface stress, which is not observed here. Moreover, the periodic boundary conditions which we apply to a small surface cell may exert a constraint on the extended network of Si–O bonds and result in an overestimation of the calculated stress. However, this is not expected to affect either the observed stress evolution or the local environment of impurity atoms substituted into the oxide layer, which will be investigated in section 6.

The average Si–O bond in the fully oxidised structure is 3% longer than in the absence of surface stress, at a coverage of 0.75 ML. This has been shown to drive dissociative water adsorption on the native oxide layer [34]. Namely, stretching of the Si–O bond leads to a decrease in the Si d orbital occupancies, allowing donation of water lone pairs onto electrophilic Si sites. Dissociative water adsorption promotes breaking of Si–O bonds in the oxide layer, exposes reactive sites and thus facilitates further oxidation reactions [34].

5 Impurity Segregation at Low Doping Concentration

Before investigating the energetics of dopant substitution close to the Si(100) surface, single neutral P and B impurity atoms were substituted into a 64 atom bulk supercell. The close match in atomic radii between P and Si caused a variation in bond length of less than 0.01 \AA and a negligible decrease in energy on relaxation. Inspection of the density of states (DOS) of the doped system around the Fermi energy shows the presence of donor levels near the conduction band, as expected (Fig. 4 (right)). However, while the excess electron strongly localises close to the P atom, a depletion of electron density in the bonding regions is visible from an analysis of the charge density difference with respect to bulk Si (Fig. 4 (left)). Indeed, a Mulliken population analysis reveals that the P atom actually receives some electronic charge from the surrounding atoms.

In contrast, B dopants are observed to add electron acceptor states close to the valence band and accept substantial electronic charge from the neighbouring Si atoms, as shown

in Fig. 5. B has a much smaller atomic radius than both P and Si, so the dopant’s four nearest-neighbours relax inwards by approximately 0.25 Å upon structural relaxation. The displacement of the dopant itself is negligible. Previous theoretical work [35] also found little movement of the B atom, while its nearest-neighbours relaxed inwards by 0.2 Å.

5.1 P in the Bare Surface

Starting with P dopants, we turn now to investigate the substitution of impurities close to the bare Si(100) surface. As in the bulk, P substitution into the surface layers is not accompanied by significant atomic or charge redistribution. The close match in atomic radius between Si and P means that effects due to stress are relatively unimportant, while the extra electron is mostly localised on the substitutional site. The energy changes associated with the presence of a P dopant in the first four surface layers with respect to the energy value upon substitution in the 64-atom bulk cell are shown in Fig. 6. As far as the layers immediately below the surface are concerned, the small energy changes computed reveal no net driving force for P segregation from the bulk to subsurface sites. The small differences may be explained by considering the residual strain in the $p(2 \times 2)$ reconstruction. In particular, the relative energetic stabilities of sites in the third and fourth layers appear to be correlated with the average bond length before substitution. Namely, in both layers the smaller P atom is unstable between the dimer rows, where average bond lengths are longer than the bulk Si bond length, (position B in Fig. 1), while the energy is reduced when the impurity is placed beneath the rows of dimers, where average bond lengths are compressed relative to the bulk, (position A).

A significant enhancement in stability over the bulk is obtained upon substitution of P for the upper atom of the surface dimer. Indeed, the p^3 bonding features of this site mirror the chemical environment of P in molecules such as PH_3 and PCl_3 , in which the bond angles are 94° and 100° respectively. The stability of this threefold-coordinated site is supported by STM experiments where the presence of P–Si dimers has been revealed after dissociation of phosphines and incorporation of P atoms in the (100) surface at 800 K [5].

Fig. 7 (centre) shows the environment and Mulliken charges around the P atom on the most stable substitutional site, after relaxation. As in the bulk, the population analysis reveals that the dopant receives electrons from its neighbours and, hence, the electron depletion on the down dimer atom is enhanced over the bare surface.

5.2 B in the Bare Surface

As in the case of P, two features of the B atom suggest that the minimum energy configuration will find it at, or near, the Si surface. Its small size causes a build up of stress in the Si lattice, which is reduced after segregation to surface sites, and its electron acceptor properties lead to saturation of surface dangling bonds. The energy of B dopants at low concentration as a function of depth below the Si (100) surface is shown in Fig. 6. Consistent with the evidence given by Ramamoorthy et al. [6], the minimum energy configuration corresponds to substitution into the second surface layer. As shown in Fig. 7 (right), this results in attraction of electrons onto the B subsurface atom increasing the positive charge on both neighbouring dimers. When the B atom is in the first layer the energy is only slightly higher. In this case, a large structural change is observed, in which the upper atom in the buckled dimer moves towards the surface by nearly 0.9 Å, flattening the dimer containing the impurity.

In slight contrast to the findings in [6], the energies of the substitutional defects in layers three and four are already comparable with the bulk value. As in the case of P, the small B atom is more stable on A sites relative to B sites. Below the second layer, there is good correlation between the average bond length before substitution and the relative energies of the B impurity on that site. However, to explain the relatively low energies on surface sites, that are actually in tension, chemical, rather than mechanical, effects must be considered. Namely, the small B atom favours sp^2 hybridisation and, indeed, the trend in energies reflects the extent to which the atoms around the impurity can relax to this structure. B is most stable in the second layer, less stable in the first layer, where the bond angles are further from the ideal 120° , and least stable close to the bulk where the

configuration is constrained to sp^3 bonding.

6 Impurity Segregation in the Oxidised Si(100) Surface

In this section we report the results of our study into the stability of substitutional impurities at an oxidised Si(100) surface. Our model of a thin native oxide layer on the (100) surface (Fig. 3) contains 1 Si^{4+} , 1 Si^{3+} , 6 Si^{2+} and 5 Si^+ species. Three of the atoms initially present in the first and second surface layers move below the surface and form no Si–O bonds. Stabilities of impurities in the oxidised surface were investigated by substitution and structural relaxation of the dopants on all 16 of these sites.

6.1 Phosphorus in the Native Oxide

The dependence of the energy relative to the bulk substitution on the number of O neighbours is shown in Fig. 8 (left) for a single, neutral P atom. The general trend reveals a decrease in stability as the number of O nearest-neighbours increases. In other words, in the presence of a native oxide layer, P is expected to segregate preferentially to the Si side of the Si/SiO_x interface.

Substitutions onto Si^{4+} and Si^{3+} sp^3 sites are accompanied by very little relaxation. The surface tensile stress remains high and the dopants are unstable. On Si^{2+} sites there is a large spread in energies and this may be explained by observing the surface relaxation. At the most stable site, local structural rearrangements of the oxide layer leave the substituted P atom in a favourable threefold-coordinated configuration (black arrow in Fig. 9 (centre)). Other rearrangements of two other Si^{2+} sites leave the P atom sp^3 -bonded but do reduce the tensile stress in the surface, thus slightly lowering the total energy. No such large-scale rearrangements are observed when P is placed on Si^+ sites, where the stability depends only on strain at the substitutional site. Bond lengths at the most stable site are actually compressed relative to bulk Si, despite the high tensile stress in the oxide layer.

Despite the range of chemical and physical environments present in the oxide layer, none of the sites discussed above are stable with respect to bulk substitution. In contrast, the results show that segregation to any of the three non-oxidised sites at the Si/SiO_x interface would be preferred. In the two most stable configurations, P replaces one Si atom of a very strained Si–Si bond (for example, red arrow in Fig. 9 (left)). Substitution of P further increases the separation, leaving the dopant favourably coordinated by three neighbours close to an under-coordinated Si atom. These results are consistent with a similar study of the Si(100)/SiO₂ interface [9], in which it was found that all structures containing P–O bonds were unstable by at least 0.5 eV in sp³ configurations or by 0.1 eV for threefold-coordinated P, with respect to the bulk. In qualitative agreement with our finding, Dabrowski et al. also report binding energies of 0.2 eV for sp³ sites and of 1.1 eV for under-coordinated Si defect sites below the interface.

Our results imply that, at low doping concentrations, P should be expelled from the native oxide layer and pile up on the Si side of the interface. The most stable sites in our model leave an under-coordinated Si atom after substitution. It is likely that substitution at defect sites consisting of just one under-coordinated Si atom would be characterised by a higher binding energy. Also, at higher doping concentrations, substitution at the remaining under-coordinated Si site to form a pair of dopants would be expected.

6.2 Boron in the Native Oxide

The effect of substituting a B atom onto sites in the native oxide layer is to increase the tensile surface stress by 0.31 Nm⁻¹, on average, and to deplete charge density on nearest-neighbour atoms. Analysis of Mulliken charges reveals that B receives an approximately constant 0.8 electrons relative to Si, irrespective of the specific substitution site.

The trend of calculated energy values with increasing numbers of O neighbours is similar to the case of P, as shown in Fig. 8 (right). In general, segregation to the bulk is preferred to the oxide layer, especially to Si⁴⁺ and Si³⁺ sites. Despite the large size mismatch between B and Si, the large spread in energies of the Si²⁺ sites can be explained largely on the basis

of chemical (rather than mechanical) effects. As in the bare surface, the low energy sites are those that allow B to form bond angles close to ideal sp^2 bonding. In the most stable site, however, the Mulliken charge of B is $+1.25 e^-$, which corresponds to leaving fewer than two electrons on the B atom. Indeed, the resulting structure is a linear O–B–O chain, in which B is sp hybridised (blue arrow, Fig. 9 (right)). The Si^+ sites are mostly very close in energy, with the exception of the compressed site discussed in the previous subsection. The stability of this site is enhanced in the case of B since the final bond lengths are much closer to the ideal B–Si length than on any other site.

Given the stability of P at under-coordinated defect sites beneath the native oxide layer, it is perhaps surprising that B is not as stable on such sites. This may be due to formation of a Si dangling bond upon B substitution and breaking of the long Si–Si bond (dashed line in Fig. 9 (left)). To investigate this issue, we replaced the under-coordinated Si atom with a second B atom (Fig. 10). Despite this being an otherwise unstable Si^+ site, the energy of this configuration is 0.3 eV more stable than the bulk, indicating that B segregation to the native oxide interface may be enhanced by pairing of impurities.

Previous theoretical calculations of B impurities at a defect-free crystalline Si/SiO₂ interface [12] found a binding energy of 0.5 eV on the Si side of the interface, while substitution into the oxide was unstable by 2.2 eV. This is in agreement with the energy we computed for the Si^{4+} site. In the same paper, the authors find that introducing an O vacancy into the oxide allows the B atom to relax to an sp^2 configuration, but it is still unstable with respect to the bulk by approximately 0.5 eV. Lowering the energy further by terminating the resulting Si dangling bond with H, they argue that B may segregate into the oxide layer by substituting onto sites neighbouring O vacancies. Similarly, we find here that segregation of impurities is particularly favourable at under-coordinated sites on the Si side of the interface, which exist at high concentration in the native oxide surface, and that the interface may be stabilised by pairing of impurities. Moreover, despite the general trend of avoiding forming B–O bonds, we find that segregation to partially oxidised sites with compressed bond lengths may be favoured.

7 Native Oxide Growth in the Presence of Surface Dopants

In the previous section, we have performed static total energy calculations with geometry optimisation to address the energetic stability of substitutional P and B impurities in a pre-existing native oxide layer model as obtained in FPMD simulations. To substantiate the results of the static calculations we now perform a series of FPMD simulations of the oxide formation on Si(100) surfaces initially doped with either P or B. For each system, two impurity atoms have been placed in a 64-atom simulation cell, in minimum energy configurations predicted by the literature (Figs. 11a and 12a). In particular, STM experiments [5] reveal the presence of P–Si dimers at the bare surface, which we found to be more stable by approximately 0.1 eV with respect to P–P dimers. In the case of B, previous theoretical work predicts the segregation of pairs of B dopants into the second layers, joined by two surface dimers, with negligible binding energy compared with isolated impurities [6].

Initial oxygen chemisorption was investigated by placing two O₂ molecules approximately 2.7 Å above the surfaces, in the positions marked by asterisks in Figs. 11a and 12a. In the case of the P-doped surface, only one of the two molecules was attracted towards the surface and dissociated after about 440 fs of simulation time according to the hot-atom mechanism observed on bare Si surfaces [27] (Fig. 11b). The O atoms were inserted between a lower Si dimer atom and the second layer, breaking a P–Si bond. The second O₂ molecule had not adsorbed after 750 fs, when the simulation was stopped. Chemisorption occurred more quickly on the B-doped surface. After 80 fs, both molecules were within 2 Å of the surface and later dissociated spontaneously (Fig. 12b).

Fig. 11 shows further snapshots from the FPMD simulation of the oxidation of the P-doped surface until the complete adsorption of six O₂ molecules. Characteristic features of the dynamics may be summarised as follows: At low oxygen coverage, O₂ molecules bind preferentially to the Si species, while they are repelled from the surface when placed in starting positions immediately above the dopants. P–O bonds form only occasionally and

are, in part, observed to break during subsequent oxidation. At intermediate coverages, molecules placed above charged Si species readily adsorb, but not necessarily dissociate immediately (as shown in Fig. 11d). Dissociation may take place later, forming both bridging Si^{2+} species and Si^{4+} species at a coverage close to unity, as observed in [27]. In the final configuration obtained (Fig. 11f), one P dopant is bound to three Si neighbours, consistent with the thermodynamically stable position found in the static total energy calculations. The second P atom, however, is bound to two O atoms, most probably trapped in a local energy minimum. Diffusion processes inaccessible to the time-scale of our simulation may help the atom escape the oxygen coordination. However, the possibility is not excluded that such metastable structures may persist during oxidation at low temperature, such that a small number of impurities may be found on the oxide side of the Si/SiO_x interface.

The development of a thin oxide film on the B-doped surface is shown in Fig. 12. The details of the simulations are generally similar to those found in the case of the bare surface or the P-doped system described above. Hot-atom dissociation of O₂ is observed to occur rapidly at low coverages upon binding to Si atoms neighbouring the B impurities. At increasing coverage, Si^{3+} species are observed to form while the B dopants tend to adopt an sp² bonding configuration and to remain segregated beneath the native oxide layer. B–O bonds are observed to form temporarily, but never to last for more than a few fs. After reaching an oxygen coverage of approximately 1 ML, incoming oxygen molecules are observed to chemisorb to the oxide structure and to remain undissociated for a few ps, after which the simulations were stopped. In order to promote a phonon-mediated dissociation, the system is heated at a rate of 1 K per time step up to a temperature of 700 K. Following this, the thermostat is switched off and the dynamics continued microcanonically. Both molecules dissociated within 2 ps as a consequence of the annealing. The final structure obtained is shown in Fig. 12f.

For both the P-doped and B-doped surfaces the simulations were performed until an oxygen coverage of 1.5 ML was reached. The final P-doped native oxide consists of 12 O atoms bonded to 10 Si atoms, forming 30% Si^{4+} , 10% Si^{3+} , 10% Si^{2+} and 50% Si^{+} species. In the B-doped structure, 12 O atoms were bonded to 12 Si atoms, forming 8%

Si⁴⁺, 25% Si³⁺, 17% Si²⁺ and 50% Si⁺ species. These compositions may be compared with that of the native oxide layer obtained on the bare surface [27] (12 O atoms bound to 13 Si atoms, forming 8% Si⁴⁺, 8% Si³⁺, 46% Si²⁺ and 38% Si⁺) and with the results of a synchrotron-radiation photoelectron spectroscopy study of a cleaned Si(100) surface [32] (approximately 1:1 O:Si stoichiometry, forming 10% Si⁴⁺, 14% Si³⁺, 25% Si²⁺ and 51% Si⁺). During the simulations of the oxidation process, the average displacements of both P and B dopants perpendicular to the surfaces were typically 0.1 Å. The mean O atom depth is identical for the P- and B-doped systems. The P atoms lie 0.6 Å and the B atoms 2.0 Å below this mean depth. This suggests a mechanism for oxidation whereby dopant atoms remain at the Si/SiO_x interface, while a native oxide layer gradually builds up above them.

8 Summary and Conclusions

Given the importance of the electrostatic charge distribution of the natively oxidised Si surface on the mediation of the interactions of Si-based devices with their external environments, we have investigated the segregation of P and B impurities during the oxidation of a Si(100) surface. We have shown that segregation is controlled by a combination of chemical and mechanical effects. In the case of the bare surface, these are illustrated by the influence of the surface reconstruction on the stability of P and B substitutional defects. With respect to substitution in the bulk, both impurities were found to be more stable by approximately 0.6 eV on chemically favourable surface sites, and to favour subsurface sites, in which the Si–Si bonds are compressed relative to the bulk.

Within the context of impurity segregation, we have monitored the changes in chemical and mechanical environments of the surface during formation of a native oxide layer. It was found that surface tensile stress increased during this process, reaching 2.9 Nm⁻¹ for the surface saturated at a coverage of 1.5 ML. The native oxide layer contained a variety of oxidised Si species, whose Mulliken charges increase approximately linearly with the number of nearest-neighbour O atoms. Substitution of Si by P and B impurities in the native oxide layer revealed that stable substitutional sites are located immediately below

(for the case of P) or at (for the case of B) the Si/SiO_x interface. FPMD simulations of oxide growth on doped bare Si(100) surfaces confirm this general trend. Few P–O and B–O bonds were formed during the dynamics and segregation to threefold-coordinated sites was observed for both dopants. In the final structures, B is not bound to any oxygen atoms, while two P–O bonds are retained.

It is to be noted that neither a purely static nor a purely dynamic approach, by itself, is perfectly suited to simulate the real experimental situation. On the one hand, the results of static total energy calculations may not represent entirely oxidation processes at low temperature, where the oxide structures may remain in metastable configurations. On the other hand, FPMD simulations are intrinsically limited to local minimum structures of the potential energy surface. However, taken together, the agreement between the two approaches used here is remarkable given the very limited size of the studied system and the very short time addressable by the dynamical simulations. The picture emerging from our results is indicative of an oxidation mechanism whereby the oxide layer grows above those dopants initially present on the bare surface, leaving them trapped at the Si/SiO_x interface. Dopants are therefore not expected to influence substantially the electrostatic and Van der Waals interactions between natively oxidised Si surfaces and an external atmospheric or liquid environment. This is precious information for the construction of classical force fields to be used in future simulations of realistic device surfaces on a larger scale.

Acknowledgements

Computational resources were provided by the HPCx supercomputing facilities within the CUK consortium, by the HPCf Cambridge, UK, by the Zentrum für Informationsdienste und Hochleistungsrechnen, Dresden, and by the HLRS Stuttgart within the AQUOXSIM project and through the HPC-Europa project (RII3-CT-2003-506079, with the support of the European Community - Research Infrastructure Action of the FP6). LCC acknowledges support by the Alexander von Humboldt Stiftung and by the Deutschen Forschungsgemein-

schaft within the Emmy Noether Programme (CI 144/2-1). This work has been supported by the EPSRC, U.K.

References

- [1] S. Pisanec, L. Colombi Ciacchi, E. Vesselli, G. Comelli, O. Sbaizero, S. Meriani, and A. De Vita. *Acta Materialia*, 52:1237, 2004.
- [2] A. C. Richards Grayson, R. S. Shawgo, A. M. Johnson, N. T. Flynn, Y. Li, M. J. Cima, and R. Langer. *Proceedings of the IEEE*, 92:6, 2004.
- [3] L. Bacáková, E. Filová, F. Rypáček, V. Svorčík, and V. Starý. *Physiol. Res.*, 53:S35, 2004.
- [4] D. Hal Davis, C. S. Giannoulis, R. W. Johnson, and T. A. Desai. *Biomaterials*, 23:4019, 2002.
- [5] R. J. Hamers, Y. Wang, and J. Shan. *Appl. Surf. Sci.*, 107:25, 1996.
- [6] M. Ramamoorthy, E. L. Briggs, and J. Bernholc. *Phys. Rev. B*, 59:4813, 1999.
- [7] P. B. Griffin, S. W. Crowder, and J. M. Knight. *Appl. Phys. Lett.*, 67:482, 1995.
- [8] H. Sato, Y. Yanagisawa, M. Ogasawara, H. Kojima, H. Masuda, and N. Natsuaki. *J. Electrochem. Soc.*, 146:367, 1999.
- [9] J. Dabrowski, R. A. Casali, H. J. Müssig, R. Baierle, M. J. Caldas, and V. Zavodinsky. *J. Vac. Sci. Technol. B*, 18:2160, 2000.
- [10] R. Baierle, M. J. Caldas, J. Dabrowski, H. J. Müssig, and V. Zavodinsky. *Physica B*, 273:260, 1999.
- [11] W. B. Ying, Y. Mizokawa, Y. B. Yu, Y. Kamiura, M. Iida, and Kawamoto K. *Appl. Surf. Sci.*, 101:556, 1996.

- [12] M. Furuhashi, T. Hirose, H. Tsuji, M. Tachi, and K. Taniguchi. *Eur. Phys. J. Appl. Phys.*, 27:163, 2004.
- [13] R. B. Fair. *J. Electrochem. Soc.*, 144:708, 1997.
- [14] A. E. Morgan, T-Y. J. Chen, D. A. Reed, and J. E. Baker. *J. Vac. Sci. Technol. A*, 2:1266, 1984.
- [15] T. H. Buyuklimanli, C. W. Magee, J. W. Marino, and S. R. Walther. *J. Vac. Sci. Technol. B*, 24:408, 2006.
- [16] T. S. Wang, A. G. Cullis, E. J. H. Collart, A. J. Murrell, and M. A. Foad. *Appl. Phys. Lett.*, 77:3586, 2000.
- [17] K. Kimura, Y. Oota, K. Nakajima, and T. H. Buyuklimanli. *Curr. Appl. Phys.*, 3:9, 2003.
- [18] M. D. Segall, P. J. D. Lindan, M. J. Probert, C. J. Pickard, P. J. Hasnip, S. J. Clark, and M. C. Payne. *J. Phys.: Condens. Matter*, 14:2717, 2002.
- [19] J. P. Perdew, K. Burke, and M. Ernzerhof. *Phys. Rev. Lett.*, 77:3865, 1996.
- [20] M. T. Yin and M. L. Cohen. *Phys. Rev. Lett.*, 45:1004, 1980.
- [21] M. C. Payne, M. P. Teter, D. C. Allan, T. A. Arias, and J. D. Joannopoulos. *Rev. Mod. Phys.*, 64:1045, 1992.
- [22] In selected test cases, we have lowered the convergence threshold on the forces to 0.05 eV/\AA , obtaining changes in energy differences smaller than 0.05 eV . For instance, the differences in surface energy between a truncated and $p(2\times 2)$ reconstructed Si surface are 1.153 eV/atom and 1.149 eV/atom for thresholds of 0.2 eV/\AA and 0.05 eV/\AA , respectively. Moreover, the energy differences of a B impurity in the most stable substitution site with respect to the bulk are -0.75 and -0.78 eV for the two thresholds above.

- [23] M. D. Segall, R. Shah, C. J. Pickard, and M. C. Payne. *Phys. Rev. B*, 54:16317, 1996.
- [24] H. J. Monkhorst and J. D. Pack. *Phys. Rev. B*, 13:5188, 1976.
- [25] P. Krüger and J. Pollmann. *Phys. Rev. Lett.*, 74:1155, 1995.
- [26] C. Z. Wang, B. C. Pan, and K. M. Ho. *J. Phys. Condens. Matter*, 11:2043, 1998.
- [27] L. Colombi Ciacchi and M. C. Payne. *Phys. Rev. Lett.*, 95:196101, 2005.
- [28] D. Vanderbilt. *Phys. Rev. Lett.*, 59:1456, 1987.
- [29] Y. Miyamoto. *Phys. Rev. B*, 49:1947, 1994.
- [30] W. Haiss. *Rep. Prog. Phys.*, 64:591, 2001.
- [31] F. K. Men, W. E. Packard, and M. B. Webb. *Phys. Rev. Lett.*, 61:2469, 1988.
- [32] Y. Hoshino, T. Nishimura, T. Nakada, H. Namba, and Y. Kido. *Surf. Sci.*, 488:249, 2001.
- [33] D. Sander and H. Ibach. *Phys. Rev. B*, 43:4263, 1991.
- [34] L. Colombi Ciacchi, J. Bagdahn, D.J. Cole, M. C. Payne, and P. Gumbsch. “stress-driven oxidation chemistry of wet silicon surfaces”, submitted for publication.
- [35] C. S. Nichols, C. G. Van de Walle, and S. T. Pantelides. *Phys. Rev. B*, 40:5484, 1989.

Figure Captions

Figure 1: The bulk-terminated (left) and $p(2 \times 2)$ -reconstructed (right) Si(100) surface. The surface atoms pair to form dimers, reducing the stress parallel to the bonds (\parallel). The relatively large bond length between the second and third layers is indicative of residual tension in this direction. The stress perpendicular (\perp) to the dimer bonds originates from the large angle between the up dimer atom and its second layer neighbours. In the third and fourth layers, atoms lying on A sites are directly beneath dimer rows, while the B sites are situated between the dimer rows.

Figure 2: Mulliken population analysis of central Si atoms with increasing number of O nearest-neighbours. Charges are multiples of the electronic charge.

Figure 3: Evolution of total surface stress, g (Nm^{-1}), during growth of an oxide layer on the $p(2 \times 2)$ -reconstructed Si(100) surface (top view) at increasing oxygen coverages, Θ (ML). O atoms are shown in red and the model supercell is represented by the dotted line. Dimer bonds between first layer atoms in the bare surface are indicated by asterisks. Adsorption sites leading to decrease of stress with respect to the bare surface are indicated by arrows (see text).

Figure 4: (left) Charge-density difference associated with the substitution of a Si atom by a P dopant in bulk Si. Positive isosurfaces, corresponding to excess electrons on the P site and neighbouring atoms, are shown in blue. Negative isosurfaces, corresponding to electron depletion in the bonding regions, are shown in red. (right) Total density of states of the system compared with bulk Si (dashed line). Donor levels are indicated by an arrow. (inset) Mulliken population analysis after structural relaxation, revealing that P receives electrons from surrounding atoms. Charges are multiples of the electronic charge.

Figure 5: As in Fig. 4, for the case of B substitution. (left) Charge-density difference with respect to bulk Si. (right) Total DOS compared with bulk Si (dashed line). Acceptor levels are indicated by an arrow. (inset) Mulliken charges (as multiples of the electronic charge) after structural relaxation.

Figure 6: Relative energy of a single, neutral, substitutional P atom (left) and B atom (right) as a function of depth below the bare Si (100) surface. In the first layer, the energy is dependent on whether the dopant is substituted into the upper or lower site of the buckled dimer. In the third and fourth layers, the A sites are situated directly beneath the dimer rows while the B sites are situated between the dimer rows. Prior to substitution, the average Si–Si bond length at an A site is shorter, and at a B site is longer, than the corresponding bulk value. The dotted line represents the energy of an impurity in the bulk, deep below the Si surface.

Figure 7: (left) Mulliken charges (multiples of the electronic charge) of selected atoms in the bare surface. Surface reconstruction is accompanied by a charge transfer from the down dimer atom to the up dimer. (centre) P segregates to the up dimer site, where the bond angles are close to 90° , and further depletes electrons from the down dimer. (right) B segregates to the second layer, where the bond angles are close to the ideal 120° for sp^2 bonding, and attracts electrons from all surrounding surface dimer atoms.

Figure 8: Relative energy of a single, neutral, substitutional P atom (left) and B atom (right) as a function of number of nearest-neighbour O in the oxide layer shown in Fig. 3. The general trend reveals a tendency to avoid forming P–O and B–O bonds. The spread in energies for a given number of nearest-neighbours may be explained by combined strain and bonding effects. The dotted line represents the energy of an impurity in the bulk, deep beneath the surface.

Figure 9: (left) 16 substitutional sites in the Si(100) native oxide layer. Two Si^{2+} sites are indicated by black and blue arrows. One Si^+ site (green arrow) is under compression and is particularly stable for both P and B dopants. The strained Si–Si bond (dashed line) means that P and B are both stable on the site beneath the oxide layer indicated by the red arrow. Both dopants move further away so that they are threefold-coordinated and leave an under-coordinated Si atom. (centre) Relaxed structure of the surface with P substituted onto the Si^{2+} site. The energy of substitution is reduced by moving to a threefold-coordinated site. (right) Relaxed structure of the surface with B substituted onto the most stable Si^{2+} site, forming a linear O–B–O chain.

Figure 10: Relaxed structure of the native oxide layer on Si(100) after double B substitution on Si sites below the oxide layer (red arrow in figure 9).

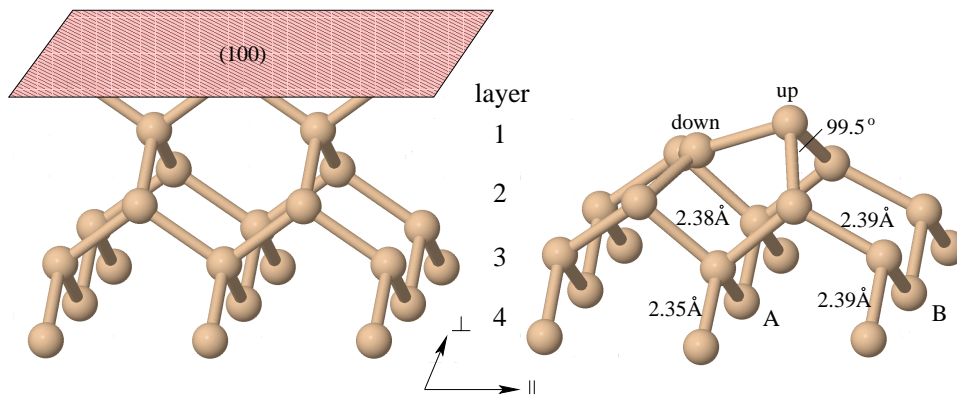
Figure 11: Side (parallel to the dimer rows) and top views of the evolution of the P-doped Si(100) surface with increasing oxygen coverage, Θ . a) Starting configuration showing pairs of P atoms (labelled 1 and 2) in upper dimer atom positions. Approximate starting positions of O_2 molecules for the subsequent simulation are indicated by asterisks.

Figure 12: Side (parallel to the dimer rows) and top views of the evolution of the B-doped Si(100) surface with increasing oxygen coverage, Θ . a) Starting configuration, showing pairs of B atoms (labelled 1 and 2) in the second layer. Approximate starting positions of O_2 molecules for the subsequent simulation are indicated by asterisks.

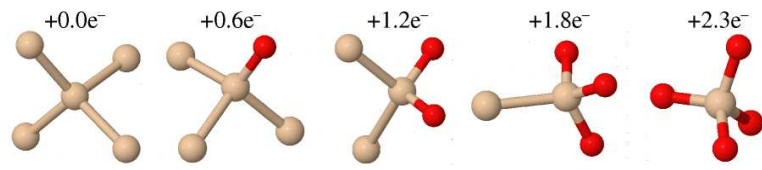
Tables

Table 1: Components of the surface stress g (Nm^{-1}) for the Si(100) surface before and after reconstruction.

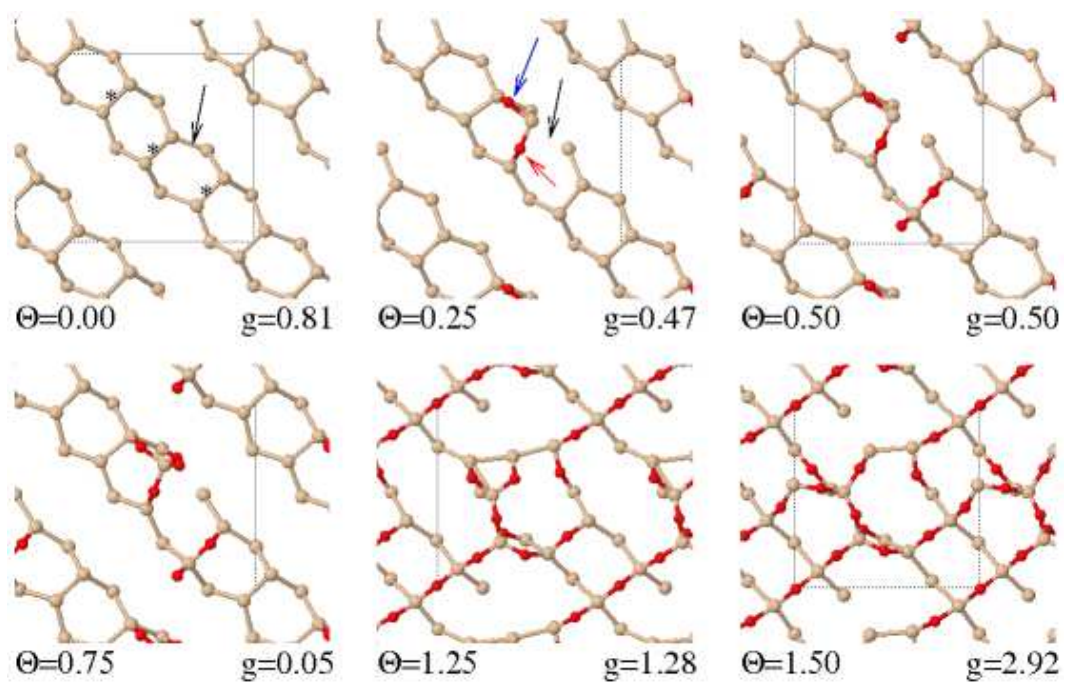
	g_{\parallel}	g_{\perp}	$g_{\parallel} - g_{\perp}$
bulk-terminated	1.78	0.32	1.46
p(2×2) (this work)	1.11	0.52	0.59
p(2×2) [29]	1.33	0.51	0.82



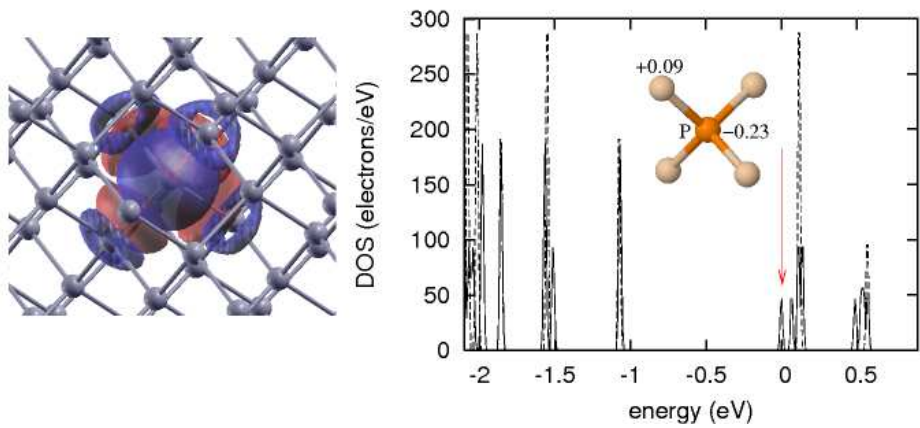
D. J. Cole, M. C. Payne, L. Colombi Ciacchi, Figure 1.



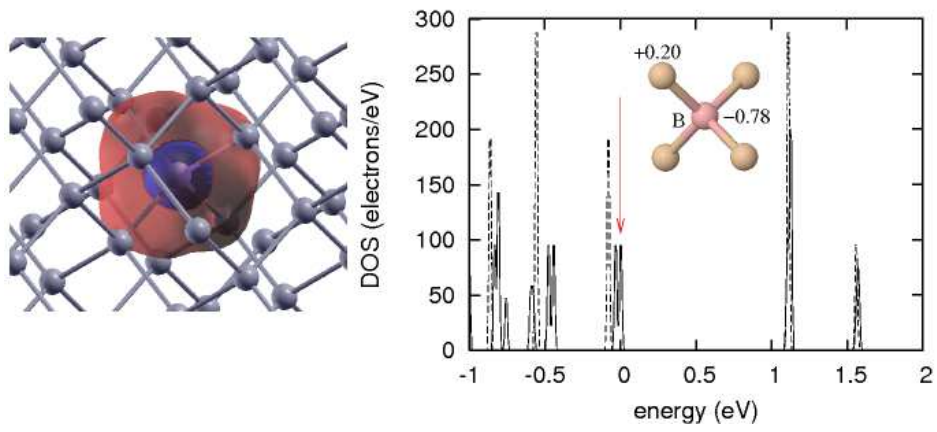
D. J. Cole, M. C. Payne, L. Colombi Ciacchi, Figure 2.



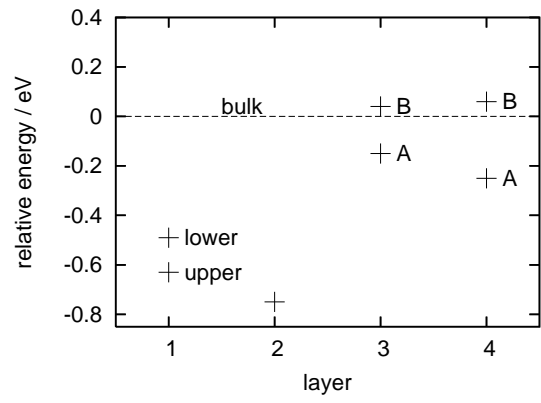
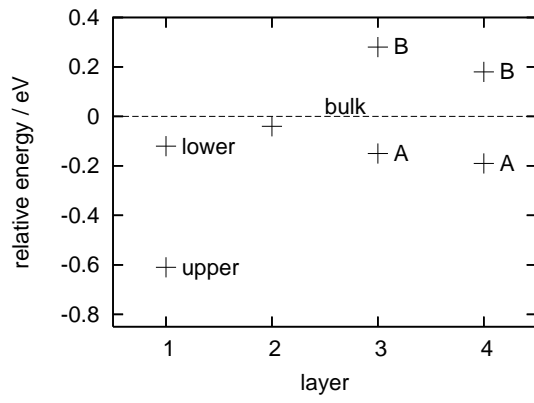
D. J. Cole, M. C. Payne, L. Colombi Ciacchi, Figure 3.



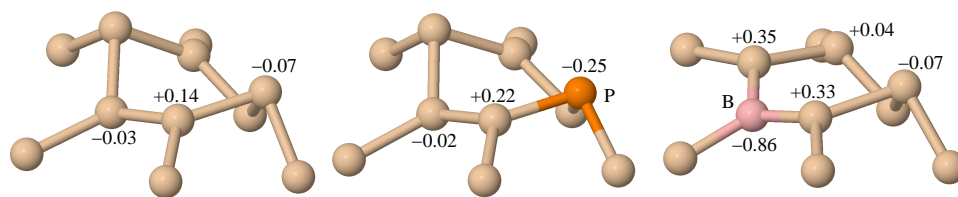
D. J. Cole, M. C. Payne, L. Colombi Ciacchi, Figure 4.



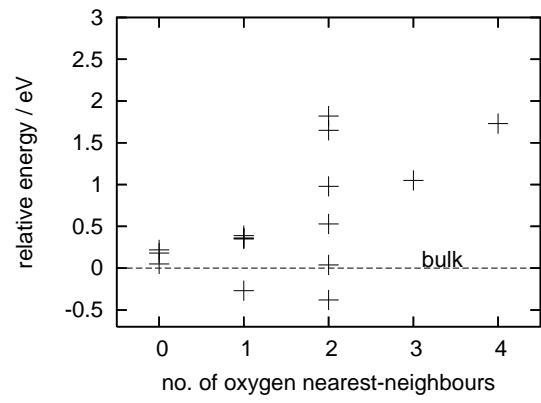
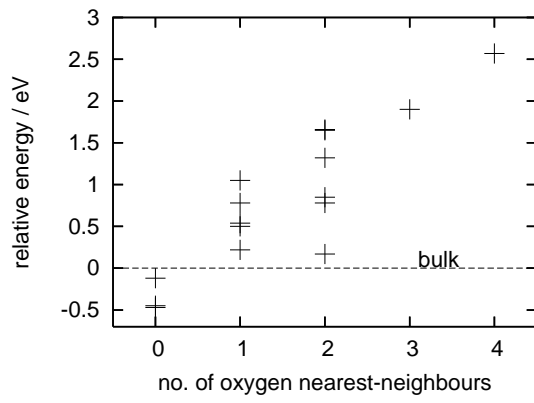
D. J. Cole, M. C. Payne, L. Colombi Ciacchi, Figure 5.



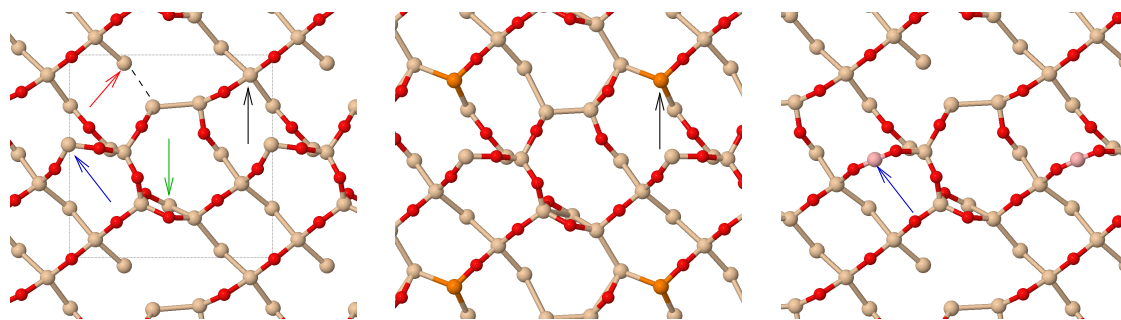
D. J. Cole, M. C. Payne, L. Colombi Ciacchi, Figure 6.



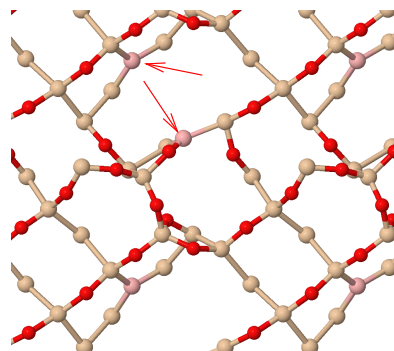
D. J. Cole, M. C. Payne, L. Colombi Ciacchi, Figure 7.



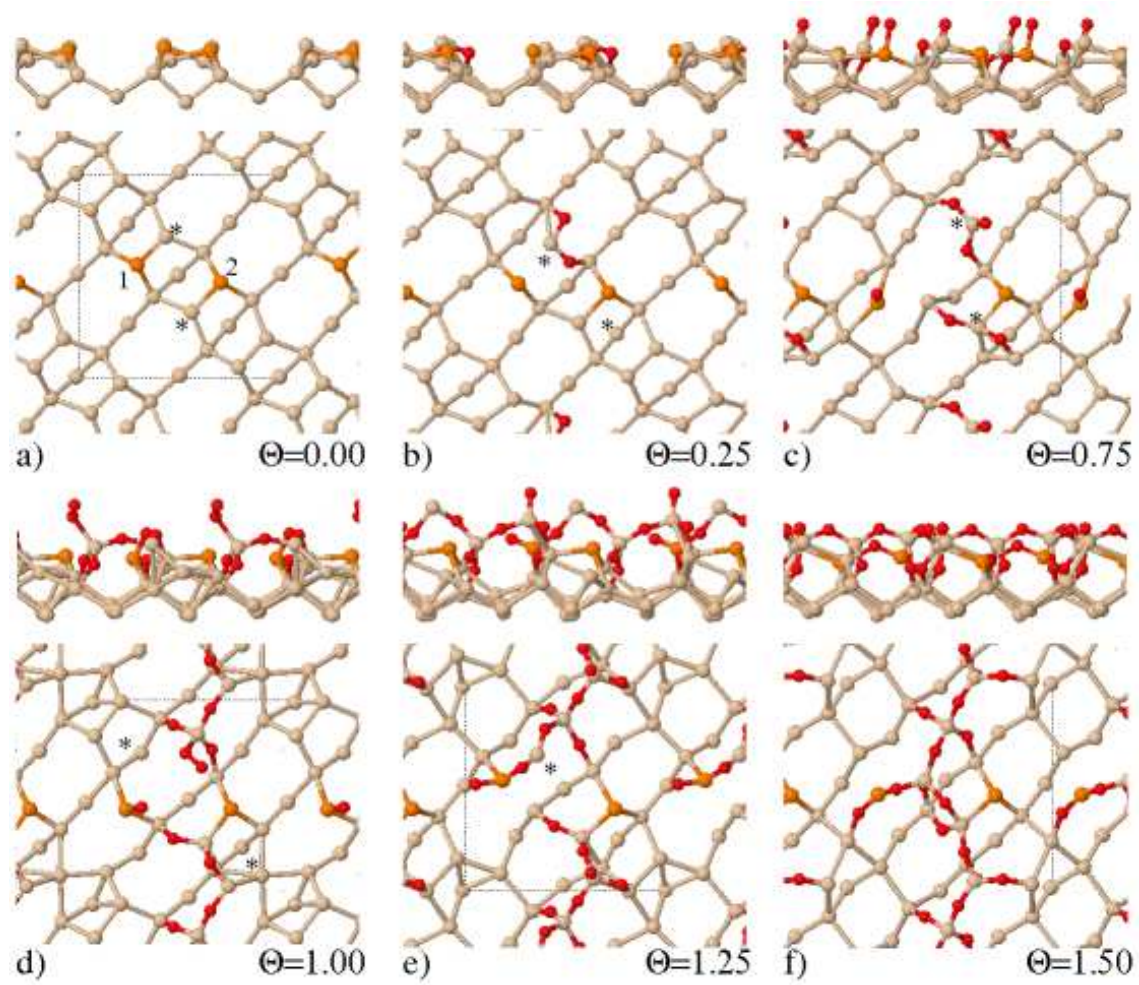
D. J. Cole, M. C. Payne, L. Colombi Ciacchi, Figure 8.



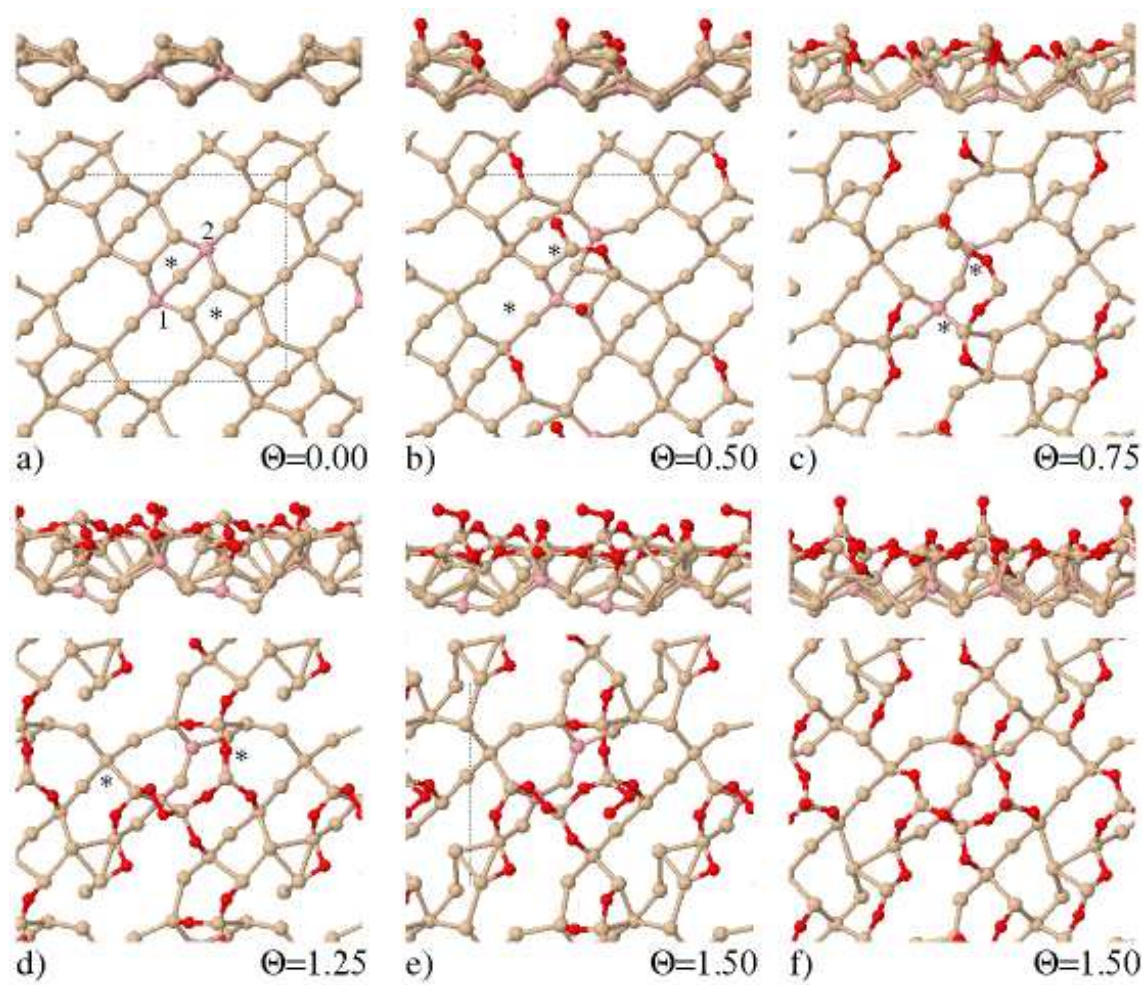
D. J. Cole, M. C. Payne, L. Colombi Ciacchi, Figure 9.



D. J. Cole, M. C. Payne, L. Colombi Ciacchi, Figure 10.



D. J. Cole, M. C. Payne, L. Colombi Ciacchi, Figure 11.



D. J. Cole, M. C. Payne, L. Colombi Ciacchi, Figure 12.